2017

Predicting Two-Phase Flow Distribution and Stability in Systems with Many Parallel Heated Channels

T Van Oevelen
Purdue University

J A. Weibel
Purdue University, jaweibel@purdue.edu

S V. Garimella
Purdue University, sureshg@purdue.edu

Van Oevelen, T; Weibel, J A.; and Garimella, S V., "Predicting Two-Phase Flow Distribution and Stability in Systems with Many Parallel Heated Channels" (2017). *CTRC Research Publications.* Paper 313.
http://dx.doi.org/10.1016/j.ijheatmasstransfer.2016.11.050

Predicting Two-Phase Flow Distribution and Stability in Systems with Many Parallel Heated Channels[1]

Tijs Van Oevelen[2], Justin A. Weibel[3], Suresh V. Garimella[4]

School of Mechanical Engineering

Purdue University, 585 Purdue Mall, West Lafayette, IN 47907 USA

Abstract

Two-phase heat exchangers are used in a variety of industrial processes in which the boiling fluid flows through a network of parallel channels. In some situations, the fluid may not be uniformly distributed through all the channels, causing a degradation in the thermal performance of the system. A methodology for modeling two-phase flow distributions in parallel-channel systems is developed. The methodology combines a pressure-drop model for individual parallel channels with a pump curve into a system flow network. Due to the non-monotonicity of the pressure drop as a function of flow rate for boiling channels, many steady-state solutions exist for the system flow equations. A new numerical approach is proposed to analyze the stability of these solutions, based on a generalized eigenvalue problem. The method is specifically designed for analyzing systems with hundreds of identical parallel channels.

The method is first applied to analyze the flow distribution and stability behavior in two-channel and five-channel systems. The asymptotic behavior of the flow stability is then analyzed for increasing numbers of channels, and it is shown that the stability behavior of a system with a constant flow-rate pump curve simplifies to the stability behavior for a constant pressure-drop pump curve. A parametric study is conducted to assess the influence of inlet temperature, heat flux, and flow rate on the stability of the uniform flow distribution solution as well as on the severity of flow maldistribution. Below some critical inlet subcooling, uniform flow distribution is always stable and maldistribution does not occur, regardless of heat flux and flow rate. Above this critical inlet subcooling, there is a range of operating parameters for which uniform flow distribution is unstable. With increasing inlet subcooling, this range broadens and the severity of the associated maldistribution increases.

Keywords

Two-phase flow, microchannel, parallel channels, flow distribution, maldistribution, stability analysis

---

[1] Submitted for possible publication in *International Journal of Heat and Mass Transfer*, 2016.

[2] E-mail address: tvanoeve@purdue.edu.

[3] E-mail address: jaweibel@purdue.edu.

[4] Corresponding author, Tel.: +1 765 494 5621. E-mail address: sureshg@purdue.edu.

Nomenclature

A_c	channel cross-section area ($H_c W_c$)
A	linearized system matrix
C	Chisholm constant
c_p	specific heat capacity
D_h	hydraulic diameter ($4A_c/D_h$)
e	natural eigenvalue, Eq. (12)
$F_p(W, \Delta p)$	pump curve
F_w	volumetric wall shear force
f	friction factor
$f(W)$	channel load curve
G	mass flux (W/A_c)
$g(\lambda)$	characteristic function
H_c	channel height
h	specific enthalpy
J	relative average flow rate starvation, Eq. (21)
L_c	channel length
M	mass matrix
m	channel inertial coefficient (L_c/A_c)
N	number of parallel channels
N_{boil}	boiling number ($Q'L_c/(W_{avg}h_{fg})$)
N_{sub}	subcooling number ($(h_f-h_{in})/h_{fg}$)
N_z	number of streamwise grid cells
n	channel fraction
$P_{[0,1]}$	projection on the interval [0,1]
p	pressure
Δp	pressure drop ($p_{in} - p_{out}$)
Q'	heat input per unit length
Re	Reynolds number Eq. (39)
R_i	flow rate fraction (W_i/W)
S	slip ratio (u_g/u_f)
T	temperature
t	time coordinate
u	streamwise velocity
v	specific volume
v	eigenvector
W	flow rate
ΔW_i^-	flow rate starvation, Eq. (19)
W_c	channel width
x	vapor quality
y	vector of state variables
z	streamwise coordinate

Greek symbols

α	void fraction
β	aspect ratio (smallest of W_c/H_c or H_c/W_c)
ϵ	partial derivative of load/pump curve
δ	deviation
γ	relative finite difference step size
λ	eigenvalue
μ	dynamic viscosity

Subscript

avg	average
c	channel
eq	thermodynamic equilibrium
f	liquid
g	vapor
I/II/III	flow rate region, Figure 1
i	channel index
in	inlet
out	outlet
p	pump
sat	saturation

1. Introduction

Two-phase heat exchangers are used in a variety of industrial processes such as steam generation, air conditioning, and nuclear reactor cooling. Increased attention is being targeted at microscale two-phase heat sinks for cooling of advanced microelectronics devices used in high-performance computing clusters, power conversion systems, and radar technologies. Such two-phase flow cooling strategies allow for increased heat transfer coefficients with reduced temperature gradients as they exploit the latent heat of evaporation. However, two-phase flow instabilities may reduce heat sink performance and limit predictability and reliability. These instabilities can pose a severe impediment to industrial-scale implementation of such cooling strategies.

Two-phase flow instabilities are commonly categorized into static and dynamic instabilities [1,2]. Static instabilities occur when a disturbance causes a steady-state operating point to jump to a different operating point. Examples are the Ledinegg (excursive) instability, boiling crisis, and flow pattern transition instabilities. Dynamic instabilities occur when several physical mechanisms interact through feedback, influenced by inertia and delay. Pressure-wave (acoustic) oscillations, density-wave oscillations, and pressure-drop oscillations are the most common dynamic instabilities. Two-phase heat sinks usually comprise a large number of parallel channels to maximize the heat transfer area density. Additional instability mechanisms that may occur in these parallel channels include flow maldistribution instability and parallel-channel instability. Flow maldistribution occurs when the distribution of flow rate across parallel channels becomes non-uniform. Parallel channel instabilities constitute sustained out-of-phase channel-to-channel oscillations.

Two-phase flow instabilities have been reviewed in the literature [1-6]. A comprehensive literature review on flow maldistribution in systems with two-phase inlet mixtures, as often encountered in air conditioning systems, can be found in Ref. [7]. In those systems, the uniformity of the phase distribution in the inlet header to the different channels plays a dominant role. The focus of this work is instead on two-phase flow maldistribution in parallel-channel systems with a subcooled inlet state.

1.1. Flow maldistribution

Flow maldistribution in parallel-channel two-phase heat sinks has been observed experimentally in various studies [8-13]. Maldistribution can have several causes: asymmetrical inlet header designs, differences in channel geometry or surface properties, non-uniform heating, and the non-monotonic nature of channel pressure drop as a function of flow rate. The latter two causes are specific to the boiling flows of interest in the current work. Mechanisms underlying these two causes can be explained using Figure 1.

Figure 1 includes a schematic representation of the pressure drop across a boiling channel as a function of flow rate for a fixed uniform heat flux. This kind of curve is referred to as the channel load curve. A pump curve represents the pressure head provided by the pump as a function of flow rate. One general pump curve and two special cases, *viz.*, constant flow rate (vertical line) and constant pressure drop (horizontal line), are shown in the figure. Steady-state system operating points are at the intersections between the channel load curve and the pump curve (*e.g.*, points B, D, and F are all possible operating points when flow is supplied according to the general pump curve). In networks of parallel channels, each channel has its own load curve, but the operating points of each channel are not independent of each other. In particular, the system must satisfy mass conservation, *i.e.*, the sum of all channel flow rates must equal the total pump flow rate, and the pressure drop across each channel must be the same.

The N-shaped load curve of the heated channel is in contrast to the monotonic adiabatic channel load curve (Figure 1). At high enough flow rates, the heated channel load curve is similar to the adiabatic case because the coolant is in the liquid state throughout the full length of the channel. At lower flow rates, boiling occurs in the heated channel. The vapor generation leads to increased frictional and accelerational pressure drops, causing the load curve to deviate from the adiabatic curve. At very low flow rates, the channel is almost completely filled with vapor, and the pressure drop decreases monotonically with decreasing flow rate. This behavior introduces a local maximum (point C) and a local minimum (point E) in the load curve, allowing three regions to be distinguished based on flow rate: region I (below W_C), region II (between W_C and W_E) and region III (above W_E). These regions correspond roughly to superheated outlet, two-phase outlet, and subcooled outlet states, respectively.

It is clear from the above discussion that the channel load curve depends on the amount of heat input, since the heat input determines the thermodynamic state of the fluid in the channel. If parallel channels have different load curves because of non-uniform heating, then they must have different flow rates to match their pressure drops. As a result, non-uniform heating can cause flow maldistribution between parallel boiling channels. However, flow maldistribution can occur even if all parallel channels have the same heat flux, *i.e.*, the same load curve, as a result of the inherent non-monotonic nature of the channel load curve. Operating points in parallel channels must have the same pressure drop, but can have very different flow rates. For example, operating points A, D, and G in Figure 1 all have the same pressure drop but at very different flow rates. In a parallel array, the channels could assume some combination of these operating points, resulting in maldistribution.

Not every steady-state system operating point is practically achievable in view of the Ledinegg instability. This static instability arises from interaction between the pump and load curves in flow boiling systems. In a single-channel system, it occurs when the slope of the load curve is lower than the

slope of the pump curve. Under this condition, small disturbances cause an exponentially growing excursion from the original steady-state operating point, eventually transitioning to a different but stable operating point. For a pump supplying a constant pressure drop, the Ledinegg instability occurs when the channel load curve has a negative slope (*e.g.*, point D in Figure 1). In contrast, a single channel with a constant flow-rate pump is unconditionally stable. A comprehensive study of the Ledinegg instability was reported by Zhang *et al.* [14]. Ruspini *et al.* [15] modeled the Ledinegg instability dynamics. For systems of multiple parallel channels, the stability criterion is more complex than for the single-channel case described here. Interactions between the pump and all the channels simultaneously govern stability.

Since maldistribution causes some channels to be starved of flow relative to a uniform distribution, premature critical heat flux (CHF) can be triggered [3]. This limits the heat flux that can be safely dissipated without inducing an extreme temperature rise in the heat source. Several remedies have been proposed to suppress two-phase flow maldistribution and other (parallel-channel) instabilities: inlet restrictions [3,11,16,17], reentrant cavities [18], diverging cross-sections [19], seed bubbles [20], increased system pressure [21], self-sustained high-frequency oscillations [22], and active control of pump and/or valves [23-26]. However, these measures may not effectively suppress maldistribution specifically, may be infeasible to implement in some applications, or may increase pressure drop. It is therefore necessary to better understand the mechanistic behavior of flow maldistribution in channels with flow boiling, and develop appropriate models to allow prediction and control of flow in two-phase heat sinks.

1.2. Literature review

Whereas there is a rich literature on various kinds of two-phase flow instabilities, relatively few studies focus on modeling two-phase flow distribution with subcooled inlet flow; we review this subset of the literature here.

Flow rate distribution among parallel evaporator tubes has been studied by Akagawa *et al.* [27]. They experimentally obtained channel load curves for individual tubes experiencing flow boiling, which displayed the N-shape as in Figure 1. They also conducted experiments in parallel tube systems where the flow distribution, excursion and hysteresis phenomena, and flow instabilities were observed and recorded. In configurations of two or three parallel channels, flow rate distributions could be estimated from their individual load curves. However, some of the predicted operating points could either not be reached or needed temporary throttling of an inlet valve on one of the channels. In all channel configurations, significant deviations from uniform flow distribution could be observed when one of the individual channel load curves had a negative slope. The authors also presented a stability criterion derived from a Laplace transformation of the linearized momentum equations for the system of parallel

channels. This criterion involves the slopes of every individual load curve. It is used to explain why some operating points are stable even when one of the channels has a negative slope in the load curve. This criterion was a good predictor of which operating points could be experimentally obtained.

Natan *et al.* [28] studied flow distribution in parallel evaporator pipes and noted in their analysis the number of different flow distributions possible at a given pressure drop. Minzer *et al.* [29] used the stability criterion of Ref. [27] to predict which of these flow distributions could occur in practice, when the inlet flow rate is fixed. This prediction corresponds well with experimental observations. Later, a model was proposed that enabled transient simulations [30]. This model was validated against steady-state experimental data of flow distributions in two parallel pipes. Furthermore, the transient simulations were used to confirm the results of the linear stability analysis; whenever the operating conditions were steered into an unstable region, the flow distribution would quickly diverge from the unstable steady-state operating point and move to a different stable steady-state point. Baikin *et al.* [31] extended the work of Ref. [30] to study up to four parallel pipes. Experimentally obtained steady-state flow distributions with different combinations of heated and unheated channels were predicted by the model and stability criterion. In general, the fraction of flow to the heated channels in which boiling occurred was reduced below average. A similar study was performed [32] on two parallel channels using a model like in Ref. [30], but with higher spatial resolution. Barnea *et al.* [33] then obtained transient experimental data of flow distribution and showed qualitative agreement with this model. However, the rate of change of state variables in the experimental system was lower than the theoretical prediction. Nevertheless, the model was able to generally predict the correct paths and end points of the transients. Zhou *et al.* [34] applied the method of Refs. [30,31] to several different configurations of heated and unheated channels with four parallel channels.

The stability of parallel channel systems was studied by Zhang *et al.* [24,25] by examining the linearized dynamic system equations. Their analysis of the system dynamics revealed an interesting feature. If all parallel channel load curves had different slopes, it was found that the system was controllable and observable. This means that controlling the pump pressure is theoretically sufficient to suppress unstable behavior in the parallel channels (flow excursions or pressure-drop oscillations) and that the flow distribution can be inferred from the total flow rate. This has been demonstrated in Ref. [25] by transient simulations. However, pump control alone is insufficient when two or more channels are identical, in which case control with inlet valves is needed [24].

Manavela Chiapero *et al.* [35] studied maldistribution resulting from the multiplicity of solutions in parallel-channel heat exchangers. They used a dynamic lumped-parameter network model, incorporating upstream compressibility, to study the evolution of pressure drop and flow rate through each channel.

Steady-state solutions were deemed 'stable' when each channel operates in a positive-slope region of its load curve. Pressure-drop oscillations occurred in the unstable solutions.

While a number of methodologies have been developed in the literature for flow distribution modeling and stability analysis, the applicability of these methods and the cases investigated have been limited to a small number of channels. However, heat sinks typically have a large number of parallel channels. The present work develops a methodology for two-phase flow distribution modeling that is capable of simulating systems having a large number of identical parallel channels. A theoretical investigation of the characteristic eigenvalue problem governing the stability of the system leads to an efficient solution approach. Examples representative of microchannel heat sinks are discussed to demonstrate the methodology and study the flow maldistribution. In addition, the effect of operating parameters on the stability of flow distributions has not yet been investigated in the literature. A parametric analysis is performed to study the effects of inlet temperature, heat flux, and flow rate on the severity of flow maldistribution.

2. Methodology

This section describes a new methodology used to model the flow distribution in parallel channels experiencing flow boiling. Our approach is modified from the method used by Akagawa *et al.* [27], Minzer *et al.* [30], and Baikin *et al.* [31] to allow prediction of stable flow distributions for a larger number of channels. The critical modifications required for this purpose are emphasized throughout this section. The flow through each channel is modeled separately and coupled in a dynamic network model. All steady-state solutions of the resulting system of equations are first calculated. A linear stability analysis of the dynamic equations is then used to differentiate between stable and unstable steady-state solutions.

2.1. Dynamic flow network equations

Our analysis is based on the ideal open-loop flow network shown in Figure 2. It consists of a pump that supplies subcooled liquid into an array of parallel heated channels. The momentum equation for each channel is given by:

$$m_i \frac{dW_i}{dt} = -f_i\left(W_i\right) + \Delta p \tag{1}$$

This equation governs the time evolution of the mass flow rate W_i of a channel with index *i*. The steady-state pressure drop as a function of flow rate, *i.e.*, the channel load curve, is given by $f_i\left(W_i\right)$. The pressure-drop model used in this paper is derived in Appendix A. With an imbalance between the steady-

state pressure drop $f_i(W_i)$ and the actual pressure drop Δp, the flow rate W_i will change. The rate of change is affected by the inertial coefficient m_i, which is equal to the ratio of channel length L_c to cross-section area A_c. The actual pressure drop Δp is the same for all channels and is the same as the pressure head provided by the pump.

The pump curve is given by:

$$0 = F_p(W, \Delta p) \tag{2}$$

The implicit function $F_p(W, \Delta p)$ specifies the relation between the pump flow rate W and the pressure drop Δp.

Mass conservation dictates that the pump flow rate W must equal the sum of individual flow rates W_i:

$$0 = \left(\sum_{i=1}^{N} W_i \right) - W \tag{3}$$

where N is the number of channels and W is also referred to as the total flow rate.

The system of differential-algebraic equations (1)-(3) describes the dynamic behavior of the flow rate distribution and pressure drop in a system of parallel channels. Flow distribution predictions based on this general approach have been successfully validated experimentally in the literature [27,30,31,33].

2.2. Steady-state flow distributions

The calculation of steady flow rate distributions is performed as follows. The cumulative load curve for the array of parallel channels is calculated by summing individual flow rates at each pressure drop level Δp. In the typical N-shaped load curve of individual heated channels, the same pressure drop occurs at three different flow rates, one in each of the three flow rate regions I, II, and III. This means that the cumulative load curve consists of up to 3^N combinations of individual flow rate distributions at any given pressure drop. Therefore, the computational complexity increases exponentially with the number of channels N.

In principle, steady-state operating points are only found at the intersections of the cumulative load curve and the pump curve. However, every point on the cumulative load curve could be an operating point of the system for some arbitrary pump curve. To retain generality, we will discuss the entire cumulative load curve without narrowing to a specific pump curve.

2.3. Stability analysis

The stability of the steady-state operating points is calculated to determine if they would be realized in practice. A stability analysis is performed on the linearization of the system dynamics given by Equations (1)-(3). This linearization is given by:

$$\begin{bmatrix} m_1 & & & & \\ & \ddots & & & \\ & & m_N & & \\ & & & 0 & \\ & & & & 0 \end{bmatrix} \cdot \frac{\mathrm{d}}{\mathrm{d}t} \begin{bmatrix} \delta W_1 \\ \vdots \\ \delta W_N \\ \delta W \\ \delta(\Delta p) \end{bmatrix} = \begin{bmatrix} -\epsilon_1 & & & & 1 \\ & \ddots & & & \vdots \\ & & -\epsilon_N & & 1 \\ & & & \epsilon_W & \epsilon_{\Delta p} \\ 1 & \cdots & 1 & -1 & 0 \end{bmatrix} \cdot \begin{bmatrix} \delta W_1 \\ \vdots \\ \delta W_N \\ \delta W \\ \delta(\Delta p) \end{bmatrix} \tag{4}$$

where δ is used to denote small deviations from the steady-state operating point. The following shorthand notation for the partial derivatives is used:

$$\epsilon_i = \frac{\partial f_i}{\partial W_i}, \qquad \epsilon_W = \frac{\partial F_p}{\partial W}, \qquad \epsilon_{\Delta p} = \frac{\partial F_p}{\partial \Delta p} \tag{5}$$

Unless the pump curve sets a constant flow rate, its slope ϵ_p can be obtained as follows:

$$\epsilon_\mathrm{p} = \left.\frac{\partial \Delta p}{\partial W}\right|_\mathrm{pump} = -\frac{\epsilon_W}{\epsilon_{\Delta p}} \tag{6}$$

Otherwise, in case of a constant flow rate pump curve, the slope of the pump curve is undefined. This motivates the use of the implicit formulation for the pump curve in Equation (2) to ensure that all coefficients in the linearized system dynamics are real numbers.

Equation (4) can be written as:

$$M \frac{\mathrm{d}y}{\mathrm{d}t} = Ay \tag{7}$$

where the vector y contains all the state variables W_i, W, and Δp. Note that the matrix M is singular, which is typical of differential-algebraic equations. The stability of this system is determined by the eigenvalues λ of the following generalized eigenvalue problem [36]:

$$\lambda M v = A v \tag{8}$$

where λ is a (generalized) eigenvalue and the (generalized) eigenvector v is composed as:

$$v = \begin{bmatrix} v_{W_1} & \cdots & v_{W_N} & v_W & v_{\Delta p} \end{bmatrix}^\mathsf{T} \tag{9}$$

The system stability depends on the signs of the eigenvalues. It is stable at an operating point if the real part of every eigenvalue λ is negative. Otherwise the operating point is unstable.

The generalized eigenvalue problem is solved numerically using the MATLAB built-in eigenvalue solver to obtain a set of eigenvalues and eigenvectors. The stability is then judged based on the signs of

the eigenvalues at every possible operating point, *i.e.*, at every pressure drop level for every combination of individual channel flow rates. A numerical approach was chosen because it allows automatic application to cases with differing number of channels.

While stability analysis method is straightforward and easy to implement, the number of different flow rate combinations increases exponentially with the number of channels *N*. In addition, the size of the eigenvalue problem increases with *N* as well. This means that interrogating the behavior of systems with a large number of parallel channels is an intrinsic challenge in terms of computational complexity, which we will address in Section 4.

3. Analysis of the generalized eigenvalue problem

This section presents a theoretical analysis of the structure of the generalized eigenvalue problem (Equation (8)). This analysis aids in understanding the stability of flow distributions in parallel channels. Furthermore, these theoretical results help enable the development of an efficient approach for simulating a large number of identical parallel channels in Section 4.

The structure of the generalized eigenvalue problem depends on the pump curve. First, we will analyze the special case of a constant pressure-drop pump curve. Then, a general pump curve is considered, which is also applicable to the case of a constant flow-rate pump curve.

3.1. Constant pressure-drop pump curve

For the constant pressure-drop pump curve, the coefficient ϵ_W is zero. In Equation (4), the second-to-last row (corresponding to the pump curve) and the last column (corresponding to the variable $\delta(\Delta p)$) can be eliminated. The following special case of the eigenvalue problem emerges:

$$\begin{aligned} &\left(\lambda m_i + \epsilon_i\right) v_{W_i} = 0, \qquad \forall i \in \{1,\ldots,N\} \\ &\left(\sum_{i=1}^{N} v_{W_i}\right) - v_W = 0 \end{aligned} \tag{10}$$

This system has *N* eigenvalues λ:

$$\lambda \in \left\{ -\frac{\epsilon_i}{m_i} \right\} \tag{11}$$

The corresponding eigenvectors are given in Table 1. Note that the eigenmodes of this special case are determined by each channel independently. A constant pressure-drop pump therefore effectively decouples the behavior of each individual channel. We define the natural eigenvalues e_i of a system of parallel channels as follows:

$$e_i = -\frac{\epsilon_i}{m_i}, \qquad i \in \{1, \ldots, N\} \tag{12}$$

The natural eigenvalues e_i describe the dynamic behavior of each individual channel operating at constant pressure drop, isolated from other channels.

The stability of the system with constant pressure-drop pump curve is determined by the signs of the natural eigenvalues e_i. For stability, all natural eigenvalues need to be negative, or equivalently, the load curve of every channel must have a positive slope ϵ_i.

3.2. General pump curve

For a general pump curve, the coefficient ϵ_W is nonzero. The eigenvalue problem is as follows:

$$\begin{aligned} (\lambda m_i + \epsilon_i) v_{W_i} - v_{\Delta p} &= 0, \qquad \forall\ i \in \{1, \ldots, N\} \\ \epsilon_W v_W + \epsilon_{\Delta p} v_{\Delta p} &= 0, \\ \left(\sum_{i=1}^{N} v_{W_i} \right) - v_W &= 0 \end{aligned} \tag{13}$$

There are two kinds of solutions to this eigenvalue problem, depending on whether λ is equal to a natural eigenvalue e_i. The first kind occurs when the natural eigenvalue e_i of at least two channels is identical, *i.e.*, multiplicity of e_i is higher than one. Then, this natural eigenvalue e_i is also an eigenvalue λ of the system. The corresponding eigenvectors are given in Table 1. Note that in this kind of eigenmodes, the flow rate does not change in the channels with a different natural eigenvalue.

In the second kind of solutions, λ is not equal to a natural eigenvalue e_i. Then, $\lambda m_i + \epsilon_i$ is nonzero for every channel. The following characteristic equation is obtained by substitution of the first and second expressions of Equation (13) into the third:

$$g(\lambda) = -\frac{\epsilon_{\Delta p}}{\epsilon_W} \tag{14}$$

The characteristic function $g(\lambda)$ is defined as follows:

$$g(\lambda) = \sum_{i=1}^{N} \frac{1}{\lambda m_i + \epsilon_i} \tag{15}$$

The eigenvalues of Equation (13) are given by the roots of Equation (14). The corresponding eigenvectors are given in Table 1. In this eigenmode, the flow rate changes in all channels simultaneously. A special case occurs for a constant flow-rate pump curve, when $\epsilon_{\Delta p}$ is zero. The characteristic equation is then $g(\lambda) = 0$.

The eigenvalues of the second kind can be understood from the graph of the characteristic function $g(\lambda)$. Figure 3 shows a schematic graph of $g(\lambda)$ for a system with $N = 3$ channels. If all natural eigenvalues e_i of the system are distinct, the function $g(\lambda)$ has N poles located at the natural eigenvalues e_i. Between every pair of poles, $g(\lambda)$ has exactly one zero. This accounts for the N-1 eigenvalues for a system with a constant flow-rate pump, *i.e.*, $\epsilon_{\Delta p}/\epsilon_W = 0$. For general pump curves, the solutions of the characteristic equation (14) are obtained at the intersections of $g(\lambda)$ with a horizontal line at $-\epsilon_{\Delta p}/\epsilon_W$. This results in an additional eigenvalue to the left of the lowest natural eigenvalue e_i to form a total set of N eigenvalues; the existing eigenvalues shift to the right.

If a natural eigenvalue e_i has multiplicity higher than one, the corresponding pole locations collapse and the number of distinct poles reduces, as does the number of eigenvalues of the second kind. Simultaneously, the repeated natural eigenvalue e_i gives rise to eigenvalues of the first kind. Each vanishing eigenvalue of the second kind is replaced by a new eigenvalue of the first kind. The total number of eigenvalues λ is therefore always N (or N-1 for the constant flow-rate pump curve as an exception), regardless of the multiplicity of the natural eigenvalues e_i.

It follows from the above discussion that the stability of a system with a general pump curve or constant flow rate-pump curve can be estimated by studying the pole locations of $g(\lambda)$, *i.e.*, the natural eigenvalues e_i. Because all eigenvalues need to be negative for the system to be stable, the stability can be determined solely from the sign of the largest eigenvalue. This largest eigenvalue $\lambda^{(1)}$ lies between the two largest natural eigenvalues $e^{(1)}$ and $e^{(2)}$, with $e^{(1)} > e^{(2)}$. When $e^{(1)}$ is negative, all eigenvalues are negative and the system is definitely stable. When $e^{(1)}$ and $e^{(2)}$ are both positive, there must be a positive eigenvalue in-between and the system is definitely unstable. When $e^{(1)}$ is positive and $e^{(2)}$ is negative (*e.g.*, Figure 3), the sign of the largest eigenvalue cannot be graphically estimated and the eigenvalue problem must be solved numerically. This leads to the conclusions that the flow distribution in an array of parallel channels subject to a general pump curve or constant flow-rate pump curve: (a) is definitely stable when all channel load curves have a positive slope, (b) is definitely unstable when at least two channel load curves have a negative slope, or (c) may be stable or unstable when there is exactly

one channel load curve with a negative slope. In the last case, a flatter pump curve, *i.e.*, with higher $\epsilon_{\Delta p}/\epsilon_W$, increases $\lambda^{(1)}$ and makes the system less stable, approaching the behavior of a system with constant pressure-drop pump curve.

4. Efficient methodology for identical parallel channels

In the case of all channel load curves being identical, the methodology discussed in Section 2 can be adapted to reduce the computational complexity. The reason is two-fold: the number of distinguishable flow rate distributions is lower, and the size of the eigenvalue problem can be reduced. We consider a general pump curve. The stability for a constant pressure-drop pump curve is trivial, because it is directly determined by the natural eigenvalues e_i.

In the general case with non-identical channels, there are 3^N different flow rate distributions; each channel can operate in one of the three flow rate regions I, II, or III. However, if the channel load curves are identical, only $(N+2)(N+1)/2$ of these combinations can be distinguished from each other. This makes a significant impact on the number of combinations that needs to be calculated, especially for large *N*.

Furthermore, using the results from the theoretical analysis in Section 3, the size of the eigenvalue problem can be reduced. At every pressure-drop level, only three flow rates are possible: W_{I} in region I, W_{II} in region II, and W_{III} in region III. The channels therefore belong to one of three groups depending on their flow rate. The numbers of channels in each group are N_{I}, N_{II}, and N_{III}, respectively, and the corresponding slopes of the channel load curve are ϵ_{I}, ϵ_{II}, and ϵ_{III}. The inertial coefficient *m* is the same for all channels.

The analysis of the eigenvalue structure revealed two kinds of eigenmodes. The first kind occurs when two or more channels have the same natural eigenvalue e_i. For identical channels, this happens when the number of channels in a group is two or more. Then, an eigenvalue λ (with multiplicity) is associated with this natural eigenvalue e_i. The second kind of eigenvalues is governed by Equation (14). It follows from Table 1 that the coefficients v_{W_i} of the eigenvector are identical for channels belonging to the same flow rate group. This means that the change in flow rate of all channels in the same flow rate group is identical. Therefore, the corresponding eigenvalue problem can be significantly reduced to:

$$\lambda\begin{bmatrix} N_{\mathrm{I}}m & & & & & \\ & N_{\mathrm{II}}m & & & & \\ & & N_{\mathrm{III}}m & & & \\ & & & 0 & & \\ & & & & 0 & \end{bmatrix}\begin{bmatrix} v_{W_{\mathrm{I}}} \\ v_{W_{\mathrm{II}}} \\ v_{W_{\mathrm{III}}} \\ v_W \\ v_{\Delta p} \end{bmatrix}=\begin{bmatrix} -N_{\mathrm{I}}\epsilon_{\mathrm{I}} & & & & N_{\mathrm{I}} \\ & -N_{\mathrm{II}}\epsilon_{\mathrm{II}} & & & N_{\mathrm{II}} \\ & & -N_{\mathrm{III}}\epsilon_{\mathrm{III}} & & N_{\mathrm{III}} \\ & & & \epsilon_W & \epsilon_{\Delta p} \\ N_{\mathrm{I}} & N_{\mathrm{II}} & N_{\mathrm{III}} & -1 & 0 \end{bmatrix}\begin{bmatrix} v_{W_{\mathrm{I}}} \\ v_{W_{\mathrm{II}}} \\ v_{W_{\mathrm{III}}} \\ v_W \\ v_{\Delta p} \end{bmatrix} \tag{16}$$

Combining all eigenvalues of the first and second kind obtained by the aforementioned approach gives the same result as directly solving Equation (8), but the matrix size of Equation (16) is only 5×5 instead of (N+2)×(N+2). This enables a significant reduction in computational complexity when the number of channels N is large.

5. Results and Discussion

This section presents results obtained using the flow distribution and stability analyses developed in this work. First, the load curve of a single heated channel is discussed. This individual channel load curve is subsequently used in several case studies with multiple identical parallel channels, and also to show the asymptotic behavior for an increasing number of channels. Finally, the effects of inlet temperature, heat input, and flow rate on the stability of the uniform flow distribution as well as on the severity of maldistribution are investigated.

5.1. Single channel

The flow distribution modeling methodology is based on individual channel load curves, which determine the steady-state pressure drop Δp as a function of individual channel flow rate W_i. We use the pressure-drop model described in Appendix A and the channel parameters given in Table 2. These parameters are representative of a microchannel heat sink. The heat flux and flow rate ranges ensure laminar flow in all of the results presented.

The resulting load curve for an individual channel is shown in Figure 4. A heated and an unheated case are shown. The load curves follow the trend shown schematically in Figure 1, owing to the mechanisms described in Section 1. The three flow rate regions for this case are: region I from a flow rate of 0 mg/s to 0.27 mg/s; region II from 0.27 mg/s to 1.2 mg/s; and region III for all flow rates higher than 1.2 mg/s.

The stability of a system with a single channel is straightforward. For a constant pressure-drop pump, the flow is stable if the slope of the channel load curve is positive. This is true in regions I and III of the heated channel load curve. The flow is unstable in region II where the slope is negative. For a constant flow-rate pump, the flow is unconditionally stable.

5.2. Two identical parallel channels

The load curve for an individual boiling channel from Section 5.1 is used in a system of two identical parallel channels. The cumulative load curve is shown in Figure 5, obtained as described in Section 2. Note that the resulting graph is multivalued, *i.e.*, there is no unique pressure drop at a given total flow rate. Also, the cumulative load curve crosses itself, meaning that different flow distributions can lead to the same total flow rate W and pressure drop Δp.

The flow distribution is visualized in Figure 6 as a graph of the flow rate fraction $R_i = W_i / W$ through each channel as a function of the total flow rate. Note that the sum of the flow rate fractions over all channels equals one. The flow rate fractions of every channel and in every flow distribution are shown simultaneously. This graph again shows that several different flow distributions can occur at a given total flow rate. The flow distribution is uniform when the flow rate fraction in both channels is 50%. There is an alternative path of flow distributions in which most of the flow rate goes through one channel while flow in the other channel is significantly reduced.

The uniform flow distribution is a special case. The corresponding flow rate region combinations, *i.e.*, I+I, II+II and III+III, are indicated on the cumulative load curve in Figure 5 and occur on the horizontal line at $R_i = 0.5$ in Figure 6. Non-uniform flow distributions are possible for total flow rates W between 0.54 mg/s and 3.5 mg/s. These cases are referred to as maldistributed. They occur as combinations of channels in different flow rate regions, *viz.*, I+II, I+III, or II+III. In these cases, one channel always has a lower flow rate than the other. With respect to nominal uniform flow conditions, we can generally say that a channel with a flow rate lower than the average of all channels is starved of flow. This can be considered an unfavorable situation compared to uniform flow; the lack of flow rate can cause the fluid to evaporate to superheated vapor state at the exit and consequently reduce thermal performance.

For constant total flow rate, the stability of the steady-state operating points is assessed using the eigenvalue method explained in Section 4. The color of each operating point in Figure 5 and Figure 6 denotes the stability. Steady operation cannot be maintained at unstable points without external control. For a constant pressure drop (not indicated in Figure 5 and Figure 6), the trivial stability assessment is the same as the single-channel case, because this boundary condition effectively decouples parallel channels from one another. In the remainder of this text, stability will be assessed assuming the system operates at a fixed total flow rate, unless otherwise stated.

The stability behavior can be explained using our theoretical analysis of the eigenvalue problem in Section 3. The combinations I+I, III+III, and I+III are stable because both channels operate in a positive-

slope region. The combination II+II is unstable because both channels operate in a negative-slope region. The stability of the remaining combinations (I+II and II+III) is determined by the relative magnitudes of the individual channel load curve slopes. Combination I+II is stable because the positive load curve slope of the one channel is steeper than the negative load curve slope of the other. The opposite is true for the unstable combination II+III. These conclusions are in agreement with the criterion of Akagawa *et al.* [27].

The uniform flow distribution is unstable in combination II+II for a total flow rate W between 0.54 mg/s and 2.4 mg/s. The unfavorable maldistributed case is the only stable flow distribution over a large range of total flow rates yielding two-phase flow. Additionally, even if the uniform flow distribution is stable at a given total flow rate *W*, maldistribution can still occur as seen in the total flow rate *W* range between 2.4 mg/s and 3.5 mg/s. This indicates that maldistribution is not limited to the range where uniform distribution is unstable. Also, in such regions where multiple stable flow distributions are possible at a single total flow rate *W*, the stability analysis cannot predict which stable distribution will occur. This is commonly regarded as a hysteresis phenomenon, where the actual flow distribution depends on the transient path leading up to the operating point. This hysteresis phenomenon has also been encountered experimentally in the literature [27,29,31,33].

5.3. Five identical parallel channels

The two-channel case is the simplest parallel-channel system, and allowed a detailed explanation of the cause of maldistribution and the stability of different flow distributions. Our next example features a system with five identical heated parallel channels to illustrate the flow distribution behavior for larger numbers of channels, as in practical applications. The five-channel system is again based on the individual channel load curve from Figure 4, corresponding to the channel parameters given in Table 2.

Figure 7 presents the cumulative load curve for the five-channel system. There are clearly many more possible solutions at a fixed flow rate or pressure drop compared to the two-channel system. As in the two-channel case, the cumulative load curve crosses itself. Figure 8 shows the flow rate fractions R_i as a function of total flow rate *W*. The relative flow distribution behavior is more complicated than for the two-channel case because the number of channels and possible flow distributions is larger. The uniform flow distribution occurs when all five channels have 20% of the total flow rate. However, several flow distributions have one or more channels with much less flow rate than the others.

A pattern emerges in the stability of operating points. The stable operating points involve almost only individual channels operating in a positive-slope region, *i.e.*, I or III. Intermediate flow rates have stable operating curves that correspond to different combinations of the region I and region III curves. There is only one exception, as indicated in Figure 7. This ‘stability exception’ is a combination involving one

channel in region II and all other channels in region I that is stable for some flow rates. The results show that at most one channel can be in the negative-slope region in stable distributions. The same conclusion has been made based on the theoretical analysis of the eigenvalue problem in Section 3. Hence, the uniform flow distribution with all channels in region II, for a total flow rate W between 1.4 mg/s and 6.0 mg/s, is entirely unstable. This is a similar observation as in the two-channel case. Also, hysteresis can again be observed.

5.4. Stability behavior for increasing number of parallel channels

To further investigate the flow distribution and stability behavior for an increasing number of channels, several test cases with increasing numbers of channels N up to 200 have been simulated. Graphs of the cumulative load curve and the flow distribution as a function of total flow rate can be found in Appendix B (Supplementary Data) for the cases up to $N = 100$; once N exceeds a value of approximately 20, the results cannot be effectively visualized due to the very large number of individual lines needed to render these graphs. The stability behavior in all these cases can be summarized as follows. If all channels have a positive load curve slope, then the system is always stable. If two or more channels have a negative load curve slope, then the system is always unstable. In particular, uniform flow distribution was always found to be unstable in the negative-slope region II. If exactly one channel has a negative load curve slope, the system is sometimes stable and sometimes unstable. This agrees with our theoretical prediction (Section 3.2) that at most one channel with negative slope in the load curve occurs in the stable distributions. The stability behavior when there is exactly one negative-slope channel is determined by a "forbidden" flow rate region (contained in region II) in the individual channel load curve. If the negative-slope channel operates in this forbidden region, the system is unstable, and *vice versa*. This behavior is exemplified by the 'stability exception' that was discussed in Section 5.3 for a five-channel system (Figure 7).

The location of the forbidden region depends on the number of parallel channels N. The forbidden region for several systems with different numbers of channels is depicted in Figure 9. Note that the vertical axis uses arbitrary units for visualization purposes to offset the otherwise overlapping curves (shifted without rescaling). The bounds of the forbidden region for these cases are given in Table 3. It is clear from the data in Figure 9 and Table 3 that the location of the forbidden region converges for $N \to \infty$. In the limit, the forbidden region occupies the entire negative-slope region of the individual channel load curve.

This observation leads to the conclusion that the asymptotic limit of the stability of a system of parallel channels with constant total flow rate is determined in a straightforward fashion from the slopes of the individual channel load curves. In the limit of $N \to \infty$, the system is stable if and only if all

channels have a positive channel load curve slope, and unstable otherwise. *Remarkably, this behavior is exactly the same as for a system with constant pressure drop, as indicated in the last row of Table 3 and on Figure 9*. We conclude that the stability behavior for a system of identical parallel channels operating at constant flow rate converges asymptotically to the stability for the same system operating at constant pressure drop with an increasing number of channels.

This is an important conclusion, because it yields an approximate method for analyzing the stability of systems with many identical parallel channels for any kind of pump curve. Instead of applying the full numerical stability analysis presented in Sections 2 and 4, it is sufficient to simply look at each of the individual channel load curve slopes. As an approximate guideline, the system operating point is stable if and only if all channels have a positive load curve slope, and is otherwise unstable. The accuracy of this approximation increases with increasing number of channels, which can be estimated by the information contained in Table 3.

5.5. Parametric effects on the stability of uniform flow distribution

The stability of the uniform flow rate distribution is of primary practical concern. We pointed out in Section 5.4. that uniform flow distribution is unstable in the negative-slope region (II). The uniform distribution is stable in the positive-slope regions (I and III). This holds for any number of parallel channels higher than one, regardless of pump curve.

The flow rate range with a negative channel load curve slope, and its implications on flow distribution, is therefore crucial to the design and analysis of two-phase heat transfer systems with parallel channels. This flow rate range depends on the geometry of the channel, the fluid, and other operating conditions. Studies on the parametric dependency of boiling channel load curves in the literature to date [14,37,38] lack an assessment of the effect on the system stability (see Table 4). Therefore, we specifically characterize the extent of the negative-slope region as a function of system operating conditions. The effect of three operating parameters is considered: average channel flow rate W_{avg}, heat input Q', and inlet subcooling $\Delta T_{\text{sub}} = T_{\text{sat}} - T_{\text{in}}$. The following dimensionless numbers are used:

- The boiling number N_{boil} represents the ratio of heat input to latent heat of evaporation:

$$N_{\text{boil}} = \frac{\left(Q'L_{\text{c}}\right)/W_{avg}}{h_{\text{fg}}} = \frac{h_{\text{out}} - h_{\text{in}}}{h_{\text{fg}}} \tag{17}$$

- The subcooling number N_{sub} represents the ratio of inlet subcooling sensible heat to latent heat of evaporation:

$$N_{sub} = \frac{h_f - h_{in}}{h_{fg}} = \frac{c_{p,f}\left(T_{sat} - T_{in}\right)}{h_{fg}} \tag{18}$$

These two numbers determine the thermodynamic state of the fluid in the channel.

Figure 10(a) shows a N_{sub} - N_{boil} diagram. In this diagram, the dashed lines delineate regions in which the outlet state is saturated liquid and saturated vapor. The former is a straight line running through the origin, $N_{sub} = N_{boil}$, and the latter is a parallel line starting from $N_{boil} = 1$. All lines parallel to these two have a constant outlet quality $x_{eq,out} = N_{boil} - N_{sub}$. Figure 10(b) shows the same diagram zoomed-in on a region near the origin. The diagrams in Figure 10 also show the loci of the operating points where the slope of the channel load curve is zero for two heat flux values (1 W/m and 200 W/m). These points correspond to the local maximum and minimum of the N-shaped load curve, *i.e.*, the bounds of the negative-slope region within which the uniform flow distribution is unstable. We refer to the locus of these points as the uniform distribution stability boundary (UDSB).

The UDSB in general depends on the heat input *Q′*, but Figure 10 shows that this effect is small. This is due to the near similarity of the individual channel load curves for different heat flux values. The small deviation from perfect similarity is a result of the low accelerational pressure-drop contribution predicted by the pressure-drop model (Appendix A). The dominant pressure-drop contribution is due to viscous stress, which would result in perfectly similar channel load curves and a UDSB independent of heat flux if it was the only contribution. Also note that the UDSB for the higher heat flux appears to be discontinuous in Figure 10(b). This is due to the fact that the simulations are subject to an upper flow rate limit to avoid transition to turbulent flow, which results in a lower limit for N_{boil}, depending on the value of *Q′*. Regardless, we conclude that the uniform distribution stability boundary (UDSB) is fairly insensitive to variations in the heat flux. This allows us to interpret variations in N_{boil} either as a variation in flow rate *W* for constant heat flux *Q′*, or as a variation in heat flux *Q′* for constant flow rate *W*.

The UDSB resembles a wedge shape, originating from a point close to the origin of Figure 10. One leg is very close to the dashed line given by $N_{sub} = N_{boil}$, which corresponds to a saturated liquid outlet state. Almost as soon as a change in flow rate or heat flux causes the liquid to boil near the channel outlet, the uniform distribution becomes unstable. This is a result of the sudden vapor generation that increases the pressure drop, and causes a negative channel load curve slope. The other leg of the UDSB lies approximately at a line given by $N_{sub} = 0.2 \cdot N_{boil}$. The location of this leg of the UDSB depends on the specific case details such as channel geometry and fluid properties.

The shape of the UDSB reveals that the range of N_{boil} in which the uniform distribution is unstable increases with increasing subcooling number N_{sub}. This means that a larger difference between inlet temperature and saturation temperature causes the range of unstable uniform distribution to increase. The unstable range can extend to about $N_{\text{boil}} = 0.5$ for the highest inlet subcooling $N_{\text{sub}} = 0.1$ (corresponding to 53.6 °C inlet subcooling for water). This is a large range relative to the region with two-phase outlet states, *i.e.*, $x_{\text{eq,out}}$ between 0 and 1.

Note that the UDSB has lower bounds for N_{boil} and N_{sub} of ~0.005 and ~0.003 (corresponding to 1.6 °C inlet subcooling for water) respectively, for the case details here. When operating below one of these values, the uniform distribution is always stable, regardless of the other parameter. Importantly, the minimum of N_{sub} suggests that maldistribution should not occur in practice when the inlet temperature is sufficiently close to saturation.

5.6. Parametric effects on maldistribution severity

The effect of operating conditions on the stability of uniform flow distribution does not necessarily describe their influence on the severity of maldistribution. We first propose a metric to quantify the severity of flow maldistribution. This metric is then used to assess the effect of operating conditions on flow maldistribution severity in the limiting case where the number of channels *N* goes to infinity; this limit approximates systems with a large number of channels. Only the stable flow distributions are considered in this parametric analysis.

It has been shown for the two-channel and five-channel cases that different flow rate distributions can have the same total flow rate *W* and pressure drop Δp as a consequence of the cross-overs in the cumulative load curve. However, there are no cross-overs in the stable parts of the cumulative load curves (see Figure 5 and Figure 7). Therefore, the total flow rate *W*, or equivalently the average flow rate $W_{\text{avg}} = W/N$, and the pressure drop Δp correspond to a unique stable flow distribution. All stable flow distributions are properly parameterized by W_{avg} and Δp, and the severity of maldistribution in these cases can be represented in a Δp-W_{avg} diagram.

In order to arrive at a maldistribution metric, we first define the flow rate starvation ΔW_i^- for each channel:

$$\Delta W_i^- = \begin{cases} W_{\text{avg}} - W_i, & W_i \le W_{\text{avg}} \\ 0, & W_i > W_{\text{avg}} \end{cases} \tag{19}$$

The flow rate starvation ΔW_i^- is the amount of flow rate that channel *i* is lacking with respect to the average flow rate. Higher-than-average flow rates are considered as zero flow rate starvation; thus, ΔW_i^- is positive by definition. The average flow rate starvation is:

$$\left\langle \Delta W^- \right\rangle = \frac{1}{N}\sum_{i=1}^{N} \Delta W_i^- \tag{20}$$

As a metric to quantify the severity of maldistribution at a given operating point, we propose a relative average flow rate starvation *J*, defined by:

$$J = \frac{\left\langle \Delta W^- \right\rangle}{W_{\text{avg}}} \tag{21}$$

This metric incorporates both the amount of flow starvation of individual channels and the number of starved channels. Note that *J* quantifies the severity of maldistribution in a range between zero and one: *J* is zero for uniform flow, and *J* approaches one when the flow rate is confined to one channel, with zero flow rate in all other channels.

In order to evaluate the value of *J* in the limit for an infinite number of channels, the asymptotic flow distributions need to be retrieved from W_{avg} and Δp. As discussed in Section 5.4, there are no stable flow distributions with channels in region II in this limit. Therefore, the stable asymptotic flow distributions are completely determined by the fractions of channels, n_{I} and n_{III}, and flow rates, W_{I} and W_{III}, in the low-flow-rate region I and high-flow-rate region III, respectively. The flow rates W_{I} and W_{III} are functions only of the pressure drop Δp. These variables are related by the mass conservation equation:

$$W_{\text{avg}} = n_{\text{I}} W_{\text{I}} + n_{\text{III}} W_{\text{III}} \tag{22}$$

Using Equation (22) and $n_{\text{I}} + n_{\text{III}} = 1$, the fraction of channels in region I can be calculated from W_{avg} and Δp*:*

$$n_{\text{I}}\left(W_{\text{avg}}, \Delta p\right) = \frac{W_{\text{III}}\left(\Delta p\right) - W_{\text{avg}}}{W_{\text{III}}\left(\Delta p\right) - W_{\text{I}}\left(\Delta p\right)} \tag{23}$$

As an example, Figure 11(a) shows contours of n_{I} in a Δp-W_{avg} diagram. It is clear that a higher average flow rate W_{avg} leads to a lower fraction of channels in region I n_{I}, as follows from Equation (23). The relative average flow rate starvation J can be evaluated from W_{avg} and Δp as follows:

$$J\left(W_{\text{avg}}, \Delta p\right) = n_{\text{I}}\left(W_{\text{avg}}, \Delta p\right)\left(1 - \frac{W_{\text{I}}\left(\Delta p\right)}{W_{\text{avg}}}\right) \tag{24}$$

Figure 11(b) shows contours of the value of J in a Δp-W_{avg} diagram. Uniform distributions are found where the value of J is zero. This only occurs along two specific lines where $W_{\text{avg}} = W_{\text{I}}$ or where $W_{\text{avg}} = W_{\text{III}}$. In between these lines, and for pressure drops between the local maximum and local minimum of the N-shaped load curve, lie all stable flow distributions (which are combinations of W_{I} and W_{III}). The highest values of J (the most maldistributed cases) are found in the interior of this area. Depending on the average flow rate, the value of J decreases or increases with pressure drop.

The value of the relative average flow rate starvation J is not uniquely defined at a given W_{avg}. In order to map the dependency of relative average flow rate starvation J on the boiling number N_{boil} and subcooling number N_{sub}, we consider the best and worst cases only. These are respectively given by the minimum and maximum values of J for a given average flow rate W_{avg}. These results are depicted in the N_{sub} - N_{boil} diagram in Figure 12 for the case with parameters from Table 2. Note that the sensitivity of the result to the heat flux Q' (here 10 W/m) is again small. This is due to the similarity between channel load curves for different heat flux values, as is discussed in Section 5.5. Figure 12(a) reveals that the best case is given by the uniform distribution outside of the UDSB, where the value of relative average flow rate starvation J is zero. The J values are above zero only inside the UDSB where the uniform distribution is unstable. The worst-case maldistribution in Figure 12(b) presents a more pessimistic view. Within the UDSB, the value of J is significantly higher compared to the best case. Furthermore, even outside of the UDSB, there is an expansive region where the worst-case value of J is very high (*i.e.*, severe maldistribution). Recall that maldistribution can occur even when the uniform distribution is stable, as pointed out in Section 5.2 for the two-channel case.

The dependence of the relative average flow rate starvation J on boiling number N_{boil} and subcooling N_{sub} is qualitatively similar between the best (Figure 12(a)) and worst case (Figure 12(b)). For low N_{boil}, there is little to no maldistribution, and J increases with increasing N_{boil}. This is due to the individual channels transitioning from operating in region III to operating in region I, one channel after another. Further increase of N_{boil} eventually leads to a reduction in J as nearly all channels are operating in region I. The range of N_{boil} in which this transition happens increases with N_{sub}. Notice also that there is a region for very low values of N_{sub} where maldistribution does not occur at all.

6. Conclusions

Two-phase flow maldistribution in systems of heated parallel channels with a subcooled inlet state has been investigated. Such maldistribution can result from the non-monotonic behavior of channel pressure drop as a function of flow rate. A methodology is presented to model flow rate distributions in parallel channels. A pressure-drop model applied to every individual channel is integrated together with a pump curve into a system model. Multiple different flow distributions can occur for a given operating condition; the stability of each flow distribution is assessed by solving a generalized eigenvalue problem.

A theoretical analysis of the stability properties of systems with identical parallel channels is performed. The stability of steady-state flow distributions is dependent on the type of pump curve. For a constant pressure-drop pump curve, the stability of each individual channel is independent of the other channels. The flow in a channel is stable if and only if the slope of the channel load curve is positive. The flow distribution in a system of parallel channels is stable when all channels are at a stable operating point. For a general pump curve, the stability is determined by all channels simultaneously. It is concluded that stable flow distributions can have at most one channel with a negative slope in the channel load curve. However, one negative-slope channel load curve could make the system unstable. When all slopes are positive, the flow distribution is definitely stable. Using these theoretical results, we have developed and implemented a more efficient flow distribution and stability analysis method for systems with identical parallel channels, compared to the general approach for non-identical channels. This algorithm requires significantly less calculation time and memory, and is hence a critical enabling factor for the study of the asymptotic stability behavior for many parallel channels.

The methodology is applied to several cases with varying numbers of identical parallel boiling channels. Severe maldistribution, with several channels almost completely starved of fluid flow, can occur. Furthermore, the uniform distribution appears to be unstable for a significant flow rate range. These results indicate the potential for severe maldistribution. Additionally, the asymptotic stability behavior as the number of parallel channels increases is investigated. We demonstrate that the stability behavior for a system with constant flow-rate pump curve converges to that of the system under a constant pressure-drop condition, which is much simpler to predict. It therefore serves as a useful reference case for approximating stability if the number of channels is sufficiently large.

Finally, parametric effects of inlet subcooling, heat flux, and flow rate on the stability of the uniform distribution and on the severity of maldistribution are investigated. Using a diagram of the dimensionless boiling number N_{boil} and the subcooling number N_{sub}, we identify the operational regions where uniform flow distribution is unstable and where the severity of maldistribution is high. The severity of maldistribution is measured by a new metric, namely, the relative average flow rate starvation J. There is

a minimum inlet subcooling below which the uniform distribution is always stable and maldistribution cannot occur, regardless of the boiling number.

Acknowledgements

This material is based upon work supported by the Defense Advanced Research Projects Agency (DARPA) Microsystems Technology Office's (MTO) Intrachip/Interchip Enhanced Cooling (ICECool) Fundamentals program under Cooperative Agreement No. HR0011-13-2-0010.

The content of the information does not necessarily reflect the position or the policy of the Government, and no official endorsement should be inferred. Distribution Statement A - Approved for public release; distribution unlimited.

Appendix A. Pressure-drop model

A pressure-drop model is used to calculate the steady-state channel load curve, which is the basis for the flow distribution model discussed in Section 2. The load curve of a single channel is given by:

$$\Delta p = f\left(W\right) \tag{25}$$

The pressure-drop model is based on the separated-flow assumption with local thermal equilibrium of the phases, *i.e.*, the phases are separated from each other and have distinct properties. There can be velocity slip between the phases, but no temperature difference. We use a one-dimensional approach in which properties only change in the flow direction. Figure 13 schematically shows the channel geometry and nomenclature used.

The flow of the liquid-vapor mixture is governed by following conservation equations:

Mass conservation:

$$\frac{\partial G}{\partial z} = 0 \tag{26}$$

Momentum conservation:

$$\frac{\partial}{\partial z}\left[\left(\frac{v_{\mathrm{f}}\left(1-x\right)^2}{1-\alpha}+\frac{v_{\mathrm{g}}x^2}{\alpha}\right)G^2\right] = -\frac{\partial p}{\partial z} - F_{\mathrm{w}} \tag{27}$$

Energy conservation equation:

$$\frac{\partial}{\partial z}\left(hG\right) = \frac{Q'}{A_{\mathrm{c}}} \tag{28}$$

It is assumed that the gravitational force as well as potential and kinetic energy contributions are negligible. These assumptions are generally true for heated pipe flow in microchannels. Heating from viscous dissipation is not included for simplicity.

The primary variables in these equations are *G*, *p*, and *h*. Three boundary conditions are used to solve these first-order differential equations:

$$G\big|_{\text{inlet}} = G_{\text{in}} \tag{29}$$

$$p\big|_{\text{outlet}} = p_{\text{out}} \tag{30}$$

$$T\big|_{\text{inlet}} = T_{\text{in}} \Rightarrow h\big|_{\text{inlet}} = h\left(T_{\text{in}}, p(0)\right) \tag{31}$$

The following secondary variables are required to fully close the system of equations:

Thermodynamic equilibrium quality:

$$x_{\text{eq}} = \frac{h - h_{\text{f}}}{h_{\text{g}} - h_{\text{f}}} \tag{32}$$

The vapor quality is the same as x_{eq} but limited to the range [0,1]:

$$x = P_{[0,1]}\left(x_{\text{eq}}\right) \tag{33}$$

Void fraction:

$$\alpha = \frac{1}{1 + \frac{v_{\text{L}}}{v_{\text{V}}} S \frac{1-x}{x}} \tag{34}$$

where $S = u_{\text{g}} / u_{\text{f}}$ is the slip ratio between the vapor and liquid phases.

Empirical correlations are needed to obtain the slip ratio *S* and the frictional pressure gradient F_{w}. The slip ratio is estimated by the Zivi correlation [39]:

$$S = \left(\frac{v_{\text{g}}}{v_{\text{f}}}\right)^{\frac{1}{3}} \tag{35}$$

The frictional pressure gradient is calculated with the Lockhart-Martinelli method [40] using the correlation by Chisholm [41]. We adopt the following formulation by Muzychka and Awad [42]:

$$F_{\text{w}} = \left(\frac{\partial p}{\partial z}\right)_{\text{f}} + C\sqrt{\left(\frac{\partial p}{\partial z}\right)_{\text{f}}\left(\frac{\partial p}{\partial z}\right)_{\text{g}}} + \left(\frac{\partial p}{\partial z}\right)_{\text{g}} \tag{36}$$

The single-phase frictional pressure gradients assume that the liquid or vapor fractions of the flow occupy the entire cross-section of the channel, without the other phase being present:

$$\left(\frac{\partial p}{\partial z}\right)_{\text{f}} = 2 f_{\text{f}} \frac{v_{\text{f}} (1-x)^2 G^2}{D_{\text{h}}}, \qquad \left(\frac{\partial p}{\partial z}\right)_{\text{g}} = 2 f_{\text{g}} \frac{v_{\text{g}} x^2 G^2}{D_{\text{h}}} \tag{37}$$

The friction factor f of fully-developed laminar flow in a rectangular channel is given by [43]:

$$f = \frac{24}{\mathrm{Re}}\left(1 - 1.3553\beta + 1.9467\beta^2 - 1.7012\beta^3 + 0.9564\beta^4 - 0.2537\beta^5\right) \tag{38}$$

where β is the aspect ratio of the channel ($0 \le \beta \le 1$). The Reynolds number should be calculated based on the flow rate of each phase alone:

$$\mathrm{Re}_\mathrm{f} = \frac{(1-x)GD_\mathrm{h}}{\mu_\mathrm{f}}, \qquad \mathrm{Re}_\mathrm{g} = \frac{xGD_\mathrm{h}}{\mu_\mathrm{g}} \tag{39}$$

In Eq. (36), C is the Chisholm constant, which accounts for the interaction between the two phases. For laminar flow in both phases, its value is 5 [41].

The model is solved numerically by finite-volume discretization of the governing equations on a one-dimensional streamwise grid with N_z uniformly sized finite volumes. The number of grid cells N_z used is 10^4. The solutions of p and h are then obtained by numerical integration (using the trapezoidal rule) of the momentum and energy equations from their respective given boundary values. The continuity equation is trivially solved by $G(z) = G_\mathrm{in}$. The model uses constant fluid properties evaluated at saturation conditions at the given outlet pressure. The properties of water/steam are evaluated using CoolProp [44] in MATLAB.

The pressure drop $\Delta p = p_\mathrm{in} - p_\mathrm{out}$ is obtained from the solution by subtracting the outlet pressure from the inlet pressure. The slope of the channel load curves is approximated by forward finite differences:

$$\epsilon = \frac{f\left(W(1+\gamma)\right) - f(W)}{\gamma W} \tag{40}$$

A relative step size γ of 10^{-3} is used for all the simulations in this article. A parameter dependency study of γ was performed to verify that this choice yields accurate results.

Appendix B. Supplementary Data

Supplementary data associated with this article can be found in the online version.

References

1 J.A. Boure, A.E. Bergles, L.S. Tong, Review of Two-Phase Flow Instability, Nuclear Engineering and Design 25 (1973) 165–192.

2 L.C. Ruspini, C.P. Marcel, A. Clausse, Two-Phase Flow Instabilities: A Review, International Journal of Heat and Mass Transfer 71 (2014) 521–548.

3 A.E. Bergles, S.G. Kandlikar, On the Nature of Critical Heat Flux in Microchannels, Journal of Heat Transfer 127 (2005) 101–107.

4 L. Tadrist, Review on Two-Phase Flow Instabilities in Narrow Spaces, International Journal of Heat and Fluid Flow 28 (2007) 54–62.

5 S. Kakac, B. Bon, A Review of Two-Phase Flow Dynamic Instabilities in Tube Boiling Systems, International Journal of Heat And Mass Transfer 51 (2008) 399–433.

6 E. Manavela Chiapero, M. Fernandino, C.A. Dorao, Review on Pressure Drop Oscillations in Boiling Systems, Nuclear Engineering and Design 250 (2012) 436–447.

7 E.R. Dario, L. Tadrist, J.C. Passos, Review on Two-Phase Flow Distribution in Parallel Channels with Macro and Micro Hydraulic Diameters: Main Results, Analyses, Trends, Applied Thermal Engineering 59 (2013) 316–335.

8 G. Hetsroni, A. Mosyak, Z. Segal, E. Pogrebnyak, Two-Phase Flow Patterns in Parallel Micro-Channels, International Journal of Multiphase Flow 29 (2003) 341–360.

9 P. Balasubramanian, S.G. Kandlikar, Experimental Study of Flow Patterns, Pressure Drop, and Flow Instabilities in Parallel Rectangular Minichannels, Heat Transfer Engineering 26 (2005) 20–27.

10 D. Bogojevic, K. Sefiane, A.J. Walton, H. Lin, G. Cummins, Two-Phase Flow Instabilities in a Silicon Microchannels Heat Sink, International Journal of Heat and Fluid Flow 30 (2009) 854–867.

11 S. Szczukiewicz, N. Borhani, J.R. Thome, Two-Phase Flow Operational Maps for Multi-Microchannel Evaporators, International Journal of Heat and Fluid Flow 42 (2013) 176–189.

12 S.H. Yoon, N. Saneie, Y.J. Kim, Two-Phase Flow Maldistribution in Minichannel Heat-Sinks under Non-Uniform Heating, International Journal of Heat and Mass Transfer 78 (2014) 527–537.

13 S.N. Ritchey, J.A. Weibel, S.V. Garimella, Local Measurement of Flow Boiling Heat Transfer in an Array of Non-Uniformly Heated Microchannels, International Journal of Heat and Mass Transfer 71 (2014) 206–216.

14 T. Zhang, T. Tong, J.-Y. Chang, Y. Peles, R. Prasher, M.K. Jensen, J.T. Wen, P. Phelan, Ledinegg Instability in Microchannels, International Journal of Heat and Mass Transfer 52 (2009) 5661–5674.

15 L.C. Ruspini, C.A. Dorao, M. Fernandino, Dynamic Simulation of Ledinegg Instability, Journal of Natural Gas Science and Engineering 2 (2010) 211–216.

16 S.G. Kandlikar, W.K. Kuan, D.A. Willistein, J. Borrelli, Stabilization of Flow Boiling in Microchannels Using Pressure Drop Elements and Fabricated Nucleation Sites, Journal of Heat Transfer 128 (2006) 389–396.

17 A. Koşar, C.-J. Kuo, Y. Peles, Suppression of Boiling Flow Oscillations in Parallel Microchannels by Inlet Restrictors, Journal of Heat Transfer 128 (2006) 251–260.

18 C.-J. Kuo, Y. Peles, Flow Boiling Instabilities in Microchannels and Means for Mitigation by Reentrant Cavities, Journal of Heat Transfer 130 (2008) 072402.

19 C. T. Lu, C. Pan, A Highly Stable Microchannel Heat Sink for Convective Boiling, Journal of Micromechanics and Microengineering 19 (2009) 055013.

20 J. Xu, G. Liu, W. Zhang, Q. Li, B. Wang, Seed Bubbles Stabilize Flow and Heat Transfer in Parallel Microchannels, International Journal of Multiphase Flow 35 (2009) 773–790.

21 C.-J. Kuo, Y. Peles, Pressure Effects on Flow Boiling Instabilities in Parallel Microchannels, International Journal of Heat and Mass Transfer 52 (2009) 271–280.

22 F. Yang, X. Dai, C.-J. Kuo, Y. Peles, J. Khan, C. Li, Enhanced Flow Boiling in Microchannels by Self-Sustained High Frequency Two-Phase Oscillations, International Journal of Heat and Mass Transfer 58 (2013) 402–412.

23 Y. Taitel, U. Minzer, D. Barnea, A Control Procedure for the Elimination of Mal Flow Rate Distribution in Evaporating Flow in Parallel Pipes, Solar Energy 82 (2008) 329–335.

24 T. Zhang, J.T. Wen, A. Julius, H. Bai, Y. Peles, M.K. Jensen, Parallel-Channel Flow Instabilities and Active Control Schemes in Two-Phase Microchannel Heat Exchanger Systems, American Control Conference, Baltimore, MD, USA (2010) 3753–3758.

25 T. Zhang, J. Wen, A. Julius, Y. Peles, M.K. Jensen, Stability Analysis and Maldistribution Control of Two-Phase Flow in Parallel Evaporating Channels, International Journal of Heat and Mass Transfer 54 (2011) 5298–5305.

26 B.A. Odom, M.J. Miner, C.A. Ortiz, J.A. Sherbeck, R.S. Prasher, P.E. Phelan, Microchannel Two-Phase Flow Oscillation Control with an Adjustable Inlet Orifice, Journal of Heat Transfer 134 (2012) 122901.

27 K. Akagawa, T. Sakaguchi, M. Kono, M. Nishimura, Study on Distribution of Flow Rates and Flow Stabilities in Parallel Long Evaporators, Bulletin of the JSME 14 (1971) 837–848.

28 S. Natan, D. Barnea, Y. Taitel, Direct Steam Generation in Parallel Pipes, International Journal of Multiphase Flow 29 (2003) 1669–1683.

29 U. Minzer, D. Barnea, Y. Taitel, Evaporation in Parallel Pipes—Splitting Characteristics, International Journal of Multiphase Flow 30 (2004) 763–777.

30 U. Minzer, D. Barnea, Y. Taitel, Flow Rate Distribution in Evaporating Parallel Pipes—Modeling and Experimental, Chemical Engineering Science 61 (2006) 7249–7259.

31 M. Baikin, Y. Taitel, D. Barnea, Flow Rate Distribution in Parallel Heated Pipes, International Journal of Heat and Mass Transfer 54 (2011) 4448–4457.

32 Y. Taitel, D. Barnea, Transient Solution for Flow of Evaporating Fluid in Parallel Pipes Using Analysis Based on Flow Patterns, International Journal of Multiphase Flow 37 (2011) 469–474.

33 D. Barnea, M. Simkhis, Y. Taitel, Transient Data for Flow of Evaporating Fluid in Parallel Mini Pipes and Comparison with Theoretical Simulations, International Journal of Multiphase Flow 77 (2015) 58–64.

34 J. Zhou, S. Wang, L. Gao, L. Zhao, L. Pang, Study on Flow Instability Inside Multiple Parallel Pipes of Direct Steam Generation, International Conference on Concentrating Solar Power and Chemical Energy Systems, SolarPACES 2014, Beijing, China, Energy Procedia 69 (2015) 259–268.

35 E. Manavela Chiapero, M. Fernandino, C.A. Dorao, Mal-Distribution Phenomena Induced by Multiple Solutions in Parallel Channels Heat Exchangers, 14th International Topical Meeting on Nuclear Reactor Thermalhydraulics, NURETH-14, Toronto, Canada (2011) paper 251.

36 S. Reich, On the Local Qualitative Behavior of Differential-Algebraic Equations, Circuits, Systems and Signal Processing 14 (1995) 427–443.

37 E. Manavela Chiapero, M. Fernandino, C.A. Dorao, Parametric Study of the Pressure Characteristic Curve in a Boiling Channel, Computational Thermal Sciences 3 (2011) 157–168.

38 E. Manavela Chiapero, D. Doder, M. Fernandino, C.A. Dorao, Experimental Parametric Study of the Pressure Drop Characteristic Curve in a Horizontal Boiling Channel, Experimental Thermal and Fluid Science 52 (2014) 318–327.

39 S.M. Zivi, Estimation of Steady-State Steam Void-Fraction by Means of the Principle of Minimum Entropy Production, Journal of Heat Transfer 86 (1964) 247–251.

40 R.W., Lockhart, R.C. Martinelli, Proposed Correlation of Data for Isothermal Two-Phase, Two-Component Flow in Pipes, Chemical Engineering Progress 45 (1949) 39–48.

41 D. Chisholm, A Theoretical Basis for the Lockhart-Martinelli Correlation for Two-Phase Flow, International Journal of Heat and Mass Transfer 10 (1967) 1767–1778.

42 Y.S. Muzychka, M.M. Awad, Asymptotic Generalizations of the Lockhart-Martinelli Method for Two Phase Flows, Journal of Fluids Engineering 132 (2010) 31302.

43 R.K Shah, A.L. London, Laminar Flow Forced Convection in Ducts: A Source Book for Compact Heat Exchanger Analytical Data, Academic Press, 1978.

44 I.H. Bell, J. Wronski, S. Quoilin, V. Lemort, Pure and Pseudo-Pure Fluid Thermophysical Property Evaluation and the Open-Source Thermophysical Property Library CoolProp, Industrial and Engineering Chemistry Research 53 (2014) 2498–2508.

List of Tables

List of Figures

Figure 8. Relative flow rate distribution, shown as flow rate fraction ($R_i = W_i / W$) versus total flow rate *W*, for five identical heated parallel channels (parameters in Table 2). The stability of each operating point is judged for a system with a constant flow-rate pump.

Figure 9. Load curve of an individual channel in a system with *N* identical heated parallel channels (parameters in Table 2). The vertical axis uses arbitrary units to offset the curves for visualization (shifted without rescaling). The red color denotes the forbidden region: if any individual channel operates in this range, a system with constant flow-rate pump curve is unstable, regardless of the other channels. For comparison, the result for a system with constant pressure-drop pump curve is also shown.

Figure 10. Uniform distribution stability boundary (UDSB) in a N_{sub} - N_{boil} diagram for several values of the heat input *Q'*. (a) Full range of N_{sub} - N_{boil}, and (b) zoom-in near the origin. Channel parameters in Table 2; inlet temperature range: $T_{\text{in}} \in [45.8\ ^\circ\text{C}, 99.1\ ^\circ\text{C}]$; flow rate range: $W_{\text{avg}} \in [0\ \text{mg/s}, 60\ \text{mg/s}]$.

Figure 11. Δp-W_{avg} diagrams depicting the asymptotic limit of the flow distributions through an infinite number of identical parallel channels with contour plots of: (a) the fraction of channels in the low-flow-rate region n_{I} (yellow: no channels in region I; dark blue: all channels in region I); (b) the relative average flow rate starvation $J = n_{\text{I}}\left(1 - W_{\text{I}} / W_{\text{avg}}\right)$ (yellow: uniform distribution; dark blue: extreme maldistribution). Channel parameters are given in Table 2.

Figure 12. (a) Lowest and (b) highest possible value of the relative average flow rate starvation $J = n_{\text{I}}\left(1 - W_{\text{I}} / W_{\text{avg}}\right)$ over all stable flow distributions presented in a N_{sub} - N_{boil} diagram, overlaid by the stability boundary of uniform distribution (UDSB) for $Q' = 10$ W/m. Channel parameters in Table 2; inlet temperature range: $T_{\text{in}} \in [45.8\ ^\circ\text{C}, 99.1\ ^\circ\text{C}]$; flow rate range: $W_{\text{avg}} \in [0\ \text{mg/s}, 60\ \text{mg/s}]$.

Figure 13. Schematic channel geometry and boundary conditions.

Table 1. Summary of solutions of eigenvalue problem given by Equation (8).

Pump curve			**Eigenvalues**	**Eigenvector (corresponding to λ)**
Constant pressure drop	$\epsilon_W = 0$ $\epsilon_{\Delta p} > 0$		$\{e_i\}$	$v_{W_i} = 0, \quad \forall i : e_i \neq \lambda$ $v_W = \sum_{i=1}^{N} v_{W_i}$, $v_{\Delta p} = 0,$
General pump curve	$\epsilon_W > 0$ $\epsilon_{\Delta p} \geq 0$ ($\epsilon_{\Delta p} = 0$ for constant flow-rate pump curve)	First kind	$\{e_i \mid \text{multiplicity}(e_i) > 1\}$	$v_{W_i} = 0, \quad \forall i : e_i \neq \lambda$ $\sum_{i=1}^{N} v_{W_i} = 0,$ $v_W = v_{\Delta p} = 0,$
		Second kind	$\left\{ \lambda \left\| \sum_{i=1}^{N} \frac{1}{\lambda m_i + \epsilon_i} + \frac{\epsilon_{\Delta p}}{\epsilon_W} = 0 \right. \right\}$	$v_{W_i} = \frac{v_{\Delta p}}{\lambda m_i + \epsilon_i}$ $v_W = -\frac{\epsilon_{\Delta p}}{\epsilon_W} v_{\Delta p}$

Note: The eigenvectors are not unique. A set of linearly independent eigenvectors can be easily obtained from the conditions in the last column.

Table 2. Individual channel parameters.

Parameter	Symbol	Value
Channel width	W_c	200 μm
Channel height	H_c	200 μm
Channel length	L_c	10 mm
Fluid	-	Water
Outlet pressure	p_{out}	1 bar
Inlet temperature	T_{in}	80 °C
Heat flux	Q'	10 W/m

Table 3. Effect of the number of parallel channels on the bounds of the forbidden region in the individual channel load curve, in a system with a constant flow-rate pump. Channel parameters are given in Table 2.

Number of channels, *N*	**Lower bound of forbidden region [mg/s]**	**Upper bound of forbidden region [mg/s]**
1	-	-
2	-	-
3	0.300	0.462
4	0.288	0.571
5	0.284	0.639
7	0.278	0.711
10	0.277	0.749
20	0.273	0.976
50	0.269	1.14
100	0.269	1.17
200	0.269	1.18
Constant Δp pump curve	0.269	1.18

Table 4. Literature summary of parametric effects on the channel load curve.

Parameter	Effect	References
Heat flux Q'	Higher heat flux increases the pressure drop and shifts the local maximum and minimum in the channel load curve to higher flow rates. The relative shape of the load curve remains almost unchanged. At a given flow rate, the magnitude of the negative channel load curve slope increases for increasing heat flux at low vapor qualities; *vice versa* for high vapor qualities.	[14,37,38]
Axial heat flux distribution	With an upstream concentration of the heat flux, the negative slope of the channel load curve becomes steeper.	[37,38]
Inlet subcooling ΔT_{sub}	Increased inlet subcooling makes the negative slope in the channel load curve steeper.	[14,37,38]
System pressure p_{out}	Higher system pressure makes the magnitude of the negative channel load curve slope lower.	[14,37,38]
Type of fluid	The effect of the fluid choice is mainly determined by the reduced pressure (p/p_{crit}). See the effect of system pressure.	[14]
Hydraulic diameter D_{h}	When the hydraulic diameter decreases, the heat input and flow rate decrease at fixed heat flux and mass flux. Since the effect on flow rate is stronger, decreasing the hydraulic diameter has a similar effect as increasing the heat flux. See the effect of heat flux.	[14]
Channel length L_{c}	Increasing the channel length is similar to increasing the heat flux. See the effect of heat flux.	[14]

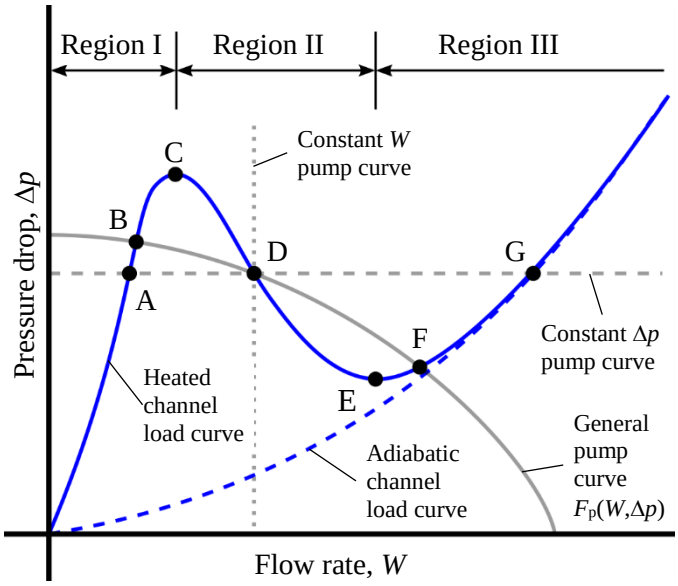

Figure 1. Diagram of pressure drop Δp versus flow rate W, including schematic pump curves as well as load curves for single adiabatic and uniformly heated channels.

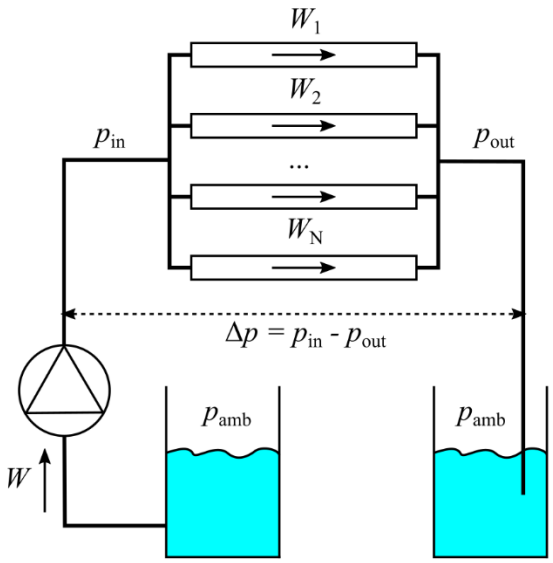

Figure 2. Schematic layout of flow through system of parallel channels.

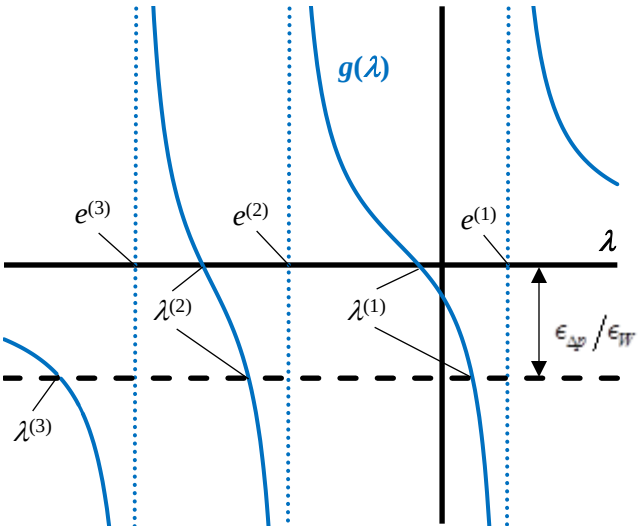

Figure 3. Schematic graph of an example characteristic function $g(\lambda)$ (see Eq. (15)), with one positive ($e^{(1)}$) and two negative ($e^{(2)}, e^{(3)}$) natural eigenvalues defining the poles. The right-hand side of the characteristic equation $g(\lambda) = -\epsilon_{\Delta p}/\epsilon_W$ is determined by the pump curve. With $\epsilon_{\Delta p}/\epsilon_W = 0$, the characteristic equation has two roots ($\lambda^{(1)}, \lambda^{(2)}$) that are both negative, despite the positive sign of $e^{(1)}$. With $\epsilon_{\Delta p}/\epsilon_W > 0$, the characteristic equation in this example has three roots: one positive ($\lambda^{(1)}$), and two negative ($\lambda^{(2)}, \lambda^{(3)}$). This example shows that the relative positive magnitude of $e^{(1)}$ and the pump curve can alter the sign of $\lambda^{(1)}$ to be either positive or negative, and demonstrates that the natural eigenvalues are insufficient to determine the sign of $\lambda^{(1)}$ when there is exactly one positive natural eigenvalue.

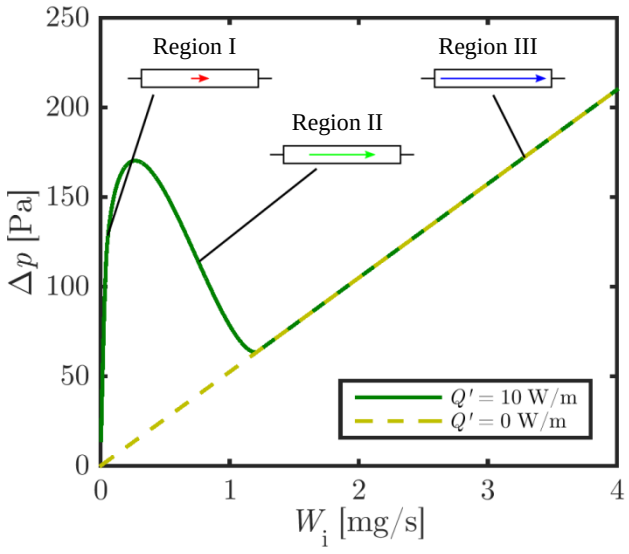

Figure 4. Pressure drop Δp versus individual-channel flow rate w_i, *i.e.*, the individual channel load curve, with and without heat input (parameters in Table 2). The three flow rate regions (defined in Figure 1) are identified with schematical channel symbols. The length (short to long) and color (red-green-blue) of the included arrows represent the magnitude of the flow rate.

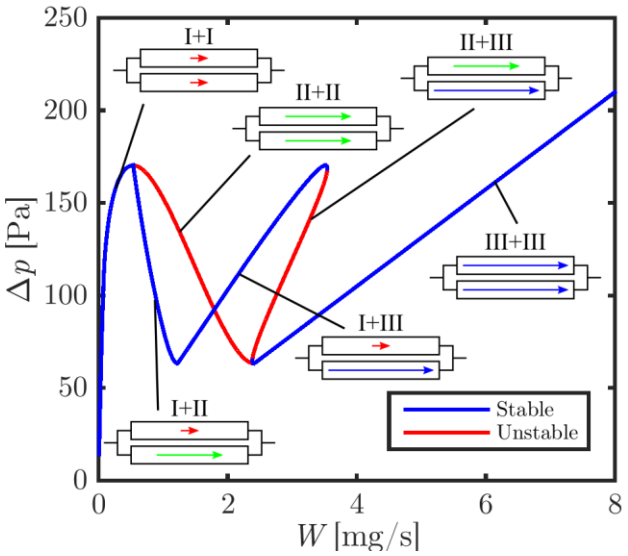

Figure 5. Pressure drop Δp versus total flow rate W, *i.e.*, the cumulative load curve, for two identical heated parallel channels (parameters in Table 2). The stability of each operating point is judged for a system with a constant flow-rate pump. The length and color of the arrows in the channel-like symbols have the same meaning as in Figure 4 to represent the flow rate combinations in the different parts of the curve.

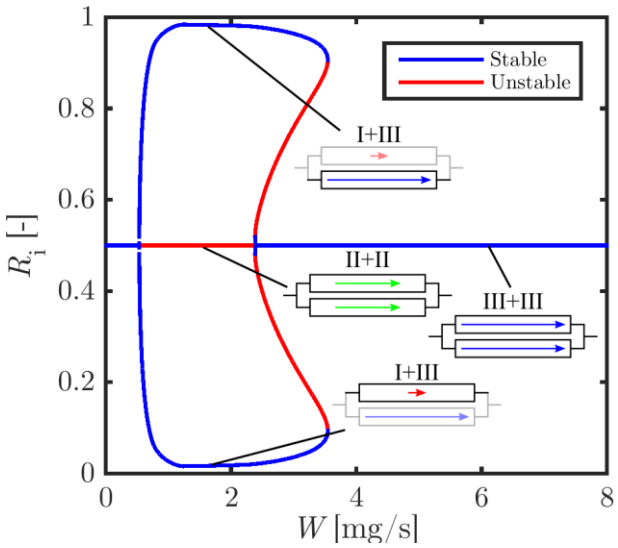

Figure 6. Relative flow rate distribution, shown as flow rate fraction ($R_i = W_i / W$), versus total flow rate W, for two identical heated parallel channels (parameters in Table 2). The stability of each operating point is judged for a system with a constant flow-rate pump. The length and color of the arrows in the channel-like symbols have the same meaning as in Figure 4 to represent the flow rate combinations in the different parts of the curve.

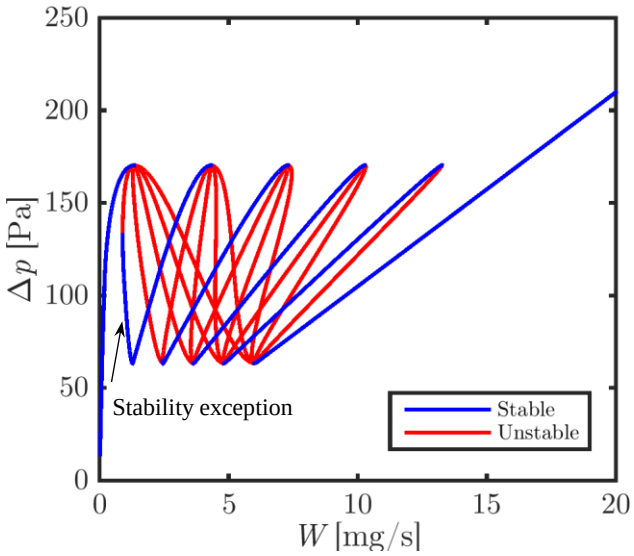

Figure 7. Pressure drop Δp versus total flow rate W, *i.e.*, cumulative load curve, for five identical heated parallel channels (parameters in Table 2). The stability of each operating point is judged for a system with a constant flow-rate pump. The 'stability exception' points to the only stable flow distribution involving a channel with flow rate in region II.

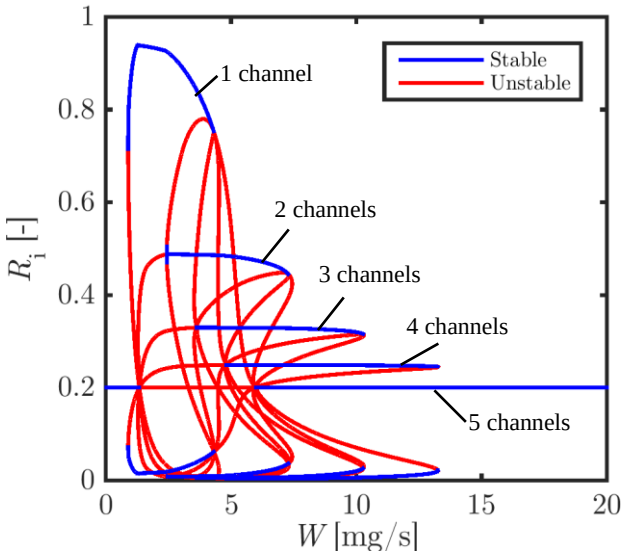

Figure 8. Relative flow rate distribution, shown as flow rate fraction ($R_i = W_i / W$) versus total flow rate W, for five identical heated parallel channels (parameters in Table 2). The stability of each operating point is judged for a system with a constant flow-rate pump.

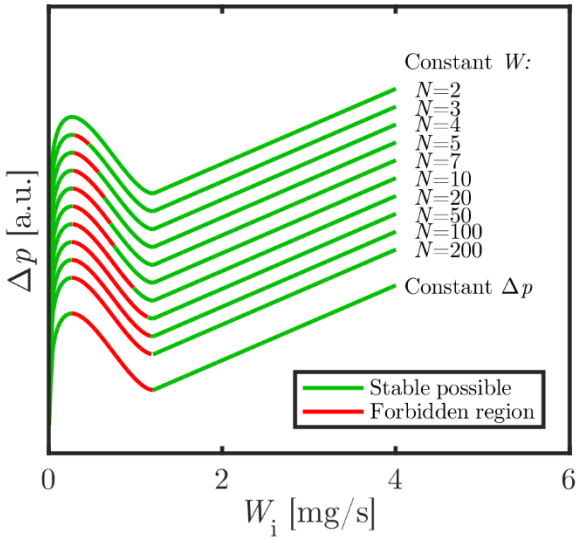

Figure 9. Load curve of an individual channel in a system with N identical heated parallel channels (parameters in Table 2). The vertical axis uses arbitrary units to offset the curves for visualization (shifted without rescaling). The red color denotes the forbidden region: if any individual channel operates in this range, a system with constant flow-rate pump curve is unstable, regardless of the other channels. For comparison, the result for a system with constant pressure-drop pump curve is also shown.

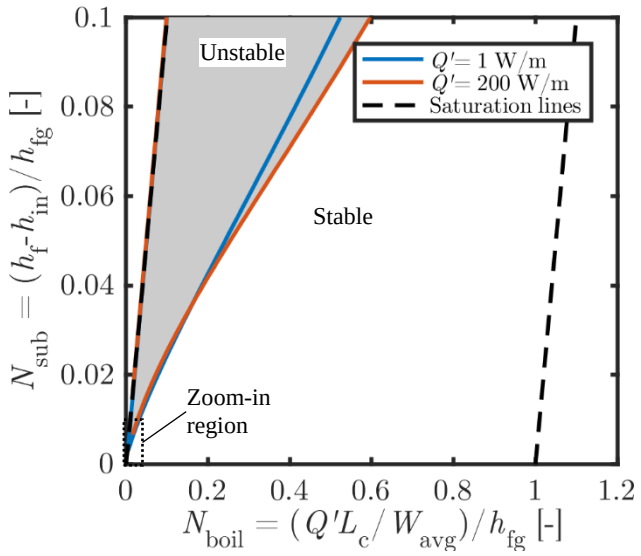

(a)

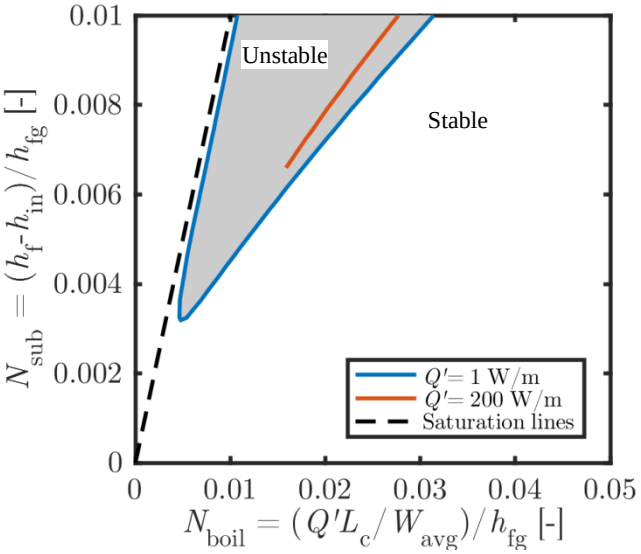

(b)

Figure 10. Uniform distribution stability boundary (UDSB) in a N_{sub} - N_{boil} diagram for several values of the heat input Q'. (a) Full range of N_{sub} - N_{boil}, and (b) zoom-in near the origin. Channel parameters in Table 2; inlet temperature range: $T_{in} \in [45.8\ °C, 99.1\ °C]$; flow rate range: $W_{avg} \in [0\ mg/s, 60\ mg/s]$.

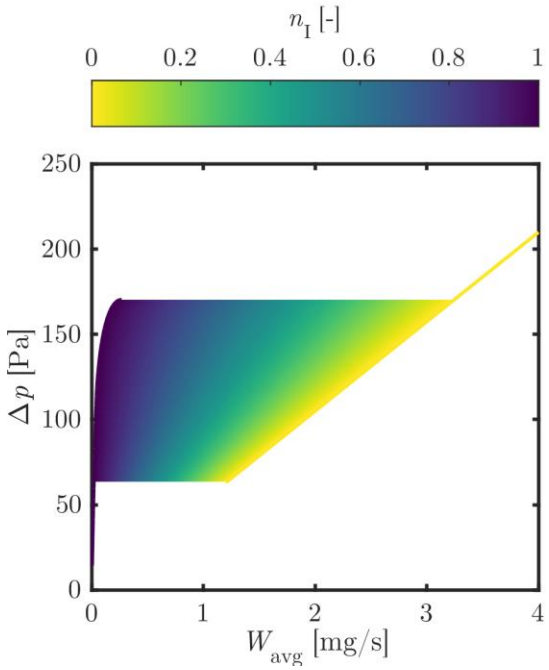

(a)

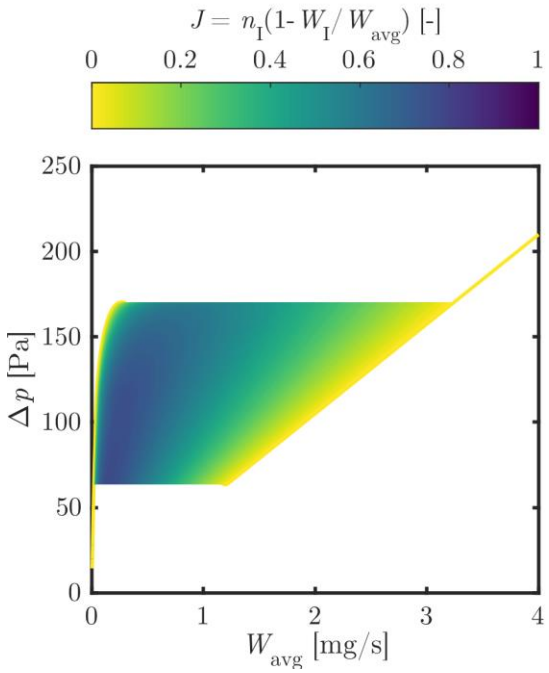

(b)

Figure 11. Δp-W_{avg} diagrams depicting the asymptotic limit of the flow distributions through an infinite number of identical parallel channels with contour plots of: (a) the fraction of channels in the low-flow-rate region n_I (yellow: no channels in region I; dark blue: all channels in region I); (b) the relative average flow rate starvation $J = n_I\left(1-W_I/W_{avg}\right)$ (yellow: uniform distribution; dark blue: extreme maldistribution). Channel parameters are given in Table 2.

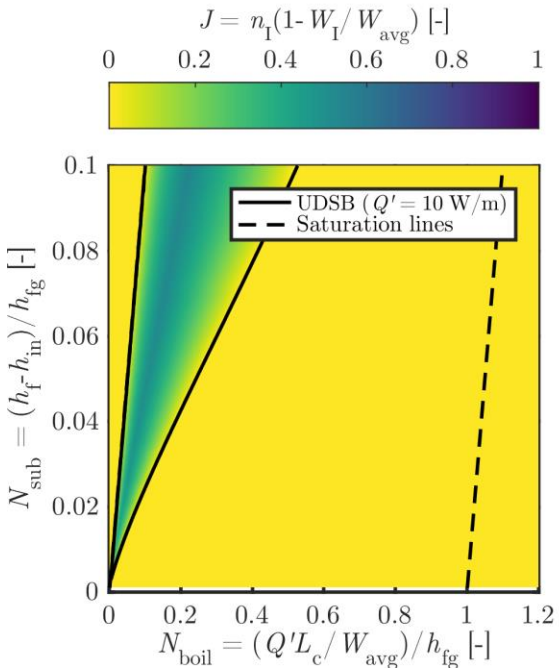

(a)

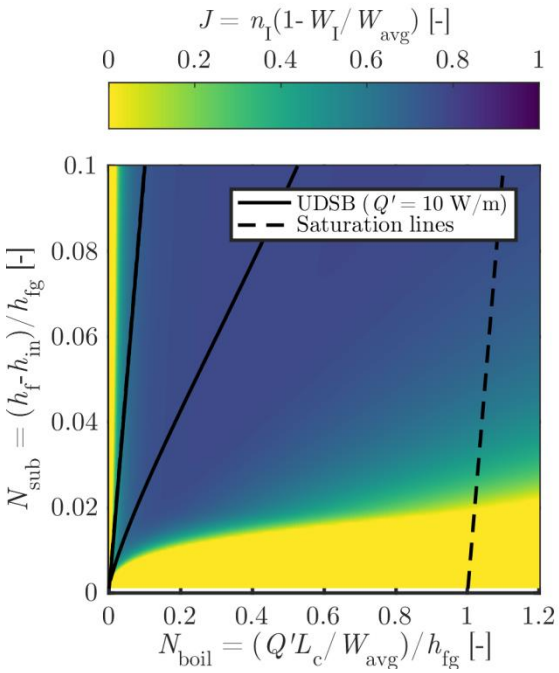

(b)

Figure 12. (a) Lowest and (b) highest possible value of the relative average flow rate starvation $J = n_{\mathrm{I}}\left(1-W_{\mathrm{I}}/W_{\mathrm{avg}}\right)$ over all stable flow distributions presented in a N_{sub} - N_{boil} diagram, overlaid by the stability boundary of uniform distribution (UDSB) for $Q' = 10$ W/m. Channel parameters in Table 2; inlet temperature range: $T_{\mathrm{in}} \in [45.8\ ^{\circ}\mathrm{C},\ 99.1\ ^{\circ}\mathrm{C}]$; flow rate range: $W_{\mathrm{avg}} \in [0\ \mathrm{mg/s},\ 60\ \mathrm{mg/s}]$.

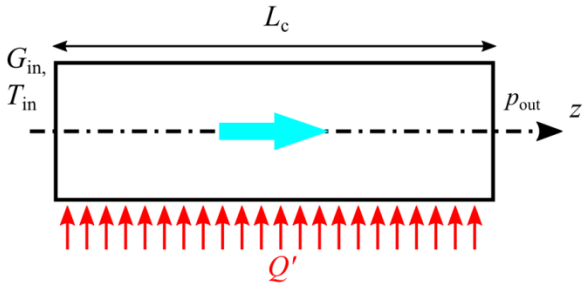

Figure 13. Schematic channel geometry and boundary conditions.